Supplemetary Information

Experimental Investigation and Bottom-up Life Cycle Assessment of Forward-osmosis Desalination Using Thermo-responsive Janus Microgels

Yuji Qin[1*], Tingting Wang[1*], Jian Zeng[1#]

[1]Sustainable Energy and Environment Thrust, The Hong Kong University of Science and Technology (Guangzhou), Nansha, Guangzhou 511400, China

[*] Equal contribution

[#] Corresponding author

E-mail addresses: jianzeng@hkust-gz.edu.cn

1. Characterization of the Janus structure with EDS , DSC , TEM and ToF-SIMS

Fig. S1. EDS mapping of Janus and uniform microgels. (a) J-3 with little P(NIPAAm) attached on the P(NIPAAm-co-SA) during the synthesis. (b) U-4 uniform microgels. (c) J-3 uniformly covered with P(NIPAAm). (d) J-3 with separated P(NIPAAm-co-SA) and P(NIPAAm) segments. shows the EDS mapping of Na element for the J-3 and U-4 microgels. As shown above, both the uniform and J-3 have Na in the chain contributed by the SA monomers. However, in the Janus microgels, the ionic P(NIPAAm-co-SA) could be covered by the P(NIPAAm) in the second step of synthesis, which does not include the Na element. Therefore, we can identify the formation of Janus structure by evaluating the Na distribution in the microgel. Fig. S1a shows the situation where the P(NIPAAm) fail to attach onto the P(NIPAAm-co-SA) part in the second synthesis step. Under this situation, the J-3 has the same chemical composition to that of U-4 and thus, Na element is distributed uniformly over the entire particle, exactly the same as for the U-4 in Fig. S1b. Fig. S1c shows the opposite situation where the P(NIPAAm) also cover the ionic segments and thus, Na element can hardly be detected on the surface. Fig. S1d display where both the P(NIPAAm) and P(NIPAAm) are exposed to the ambient under which situation we can identify a Na-concentrated (in red) and Na-less concentrated area, corresponding to the P(NIPAAm-co-SA) and P(NIPAAm), respectively. DSC thermograms collected at 5 °C/min show a single broad endothermic transition for P(NIPAAm) (T_{peak} ≈ 60.65 °C) and a systematically shifted transition for P(NIPAAm-co-SA) (T_{peak} ≈ 78.60 °C), accompanied by reduced transition enthalpy (Δ H decreases from ~109.0 to ~74.5 J/g after baseline correction). These results support the successful incorporation of SA and its enhanced hydration effect on the PNIPAAm-

related dehydration/collapse process. In the absence of heavy-metal staining, TEM/STEM contrast primarily reflects mass–thickness variations. The bright-field TEM image (Fig. S1f, left) shows a pronounced high-scattering (darker) region within the microgel, whereas the outer region exhibits weaker contrast, indicating radial heterogeneity in density/thickness. The corresponding STEM image (Fig. S1f, right) displays strong mass–thickness contrast with a mottled network-like texture, suggesting coexisting dense polymer domains and low-density regions. This radial contrast heterogeneity is consistent with the proposed core–shell architecture, comprising a denser inner core and a relatively more diffuse outer shell. When combined with the ToF-SIMS depth profiles—where PNIPAAm-related signals decrease while PSA-associated signals increase with sputter time—the outer region can be assigned to a PNIPAAm-enriched shell and the inner region to a PSA-enriched core. Note that hydrogel microgels may partially collapse or rearrange under vacuum and electron-beam irradiation; thus, TEM/STEM primarily provides qualitative structural support, while the chemical stratification is substantiated by ToF-SIMS. ToF-SIMS 3D analyses were carried out on an IONTOF M6 hybrid SIMS instrument (Ion-ToF GmbH, Münster, Germany). The analysis was performed with a 30 keV Bi_3^+ as the primary ion over an area of 150 μm × 150 μm, rastered by 10 keV Ar_{2500}^+ over an area of 400 μm × 400 μm. Charge compensation was realized using a low-energy flood gun. All SIMS spectra were analyzed using SurfaceLab 7.3. Marker ions were validated by comparing the spectra of pure PNIPAAm and pure PSA reference samples, where each ion exhibited high intensity in the corresponding reference and negligible intensity in the other.

a J-3 Janus microgel

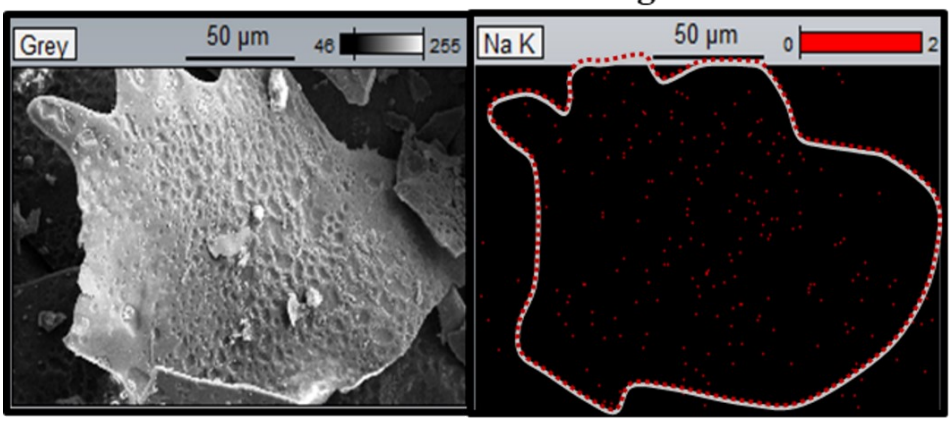

b U-4 uniform microgel

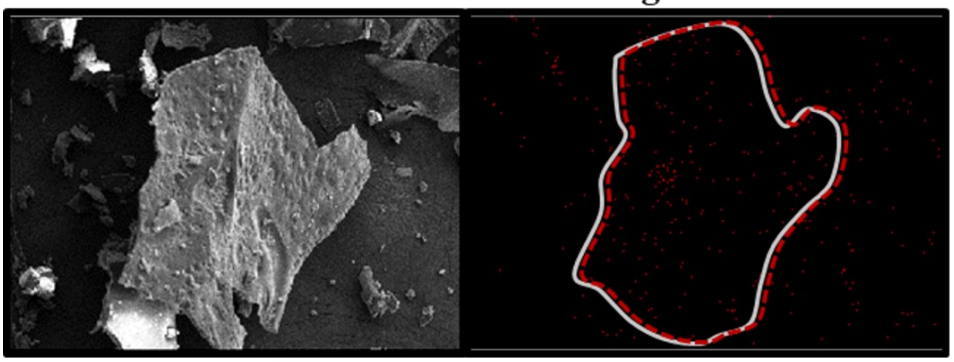

c J-3 Janus microgel

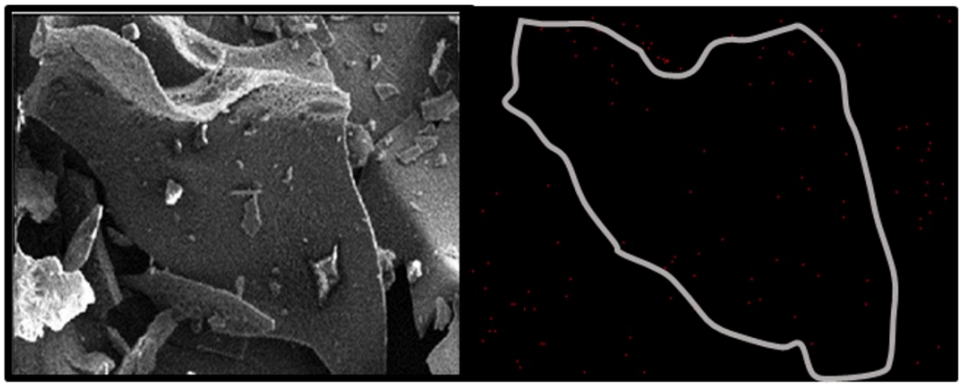

d J-3 Janus microgel

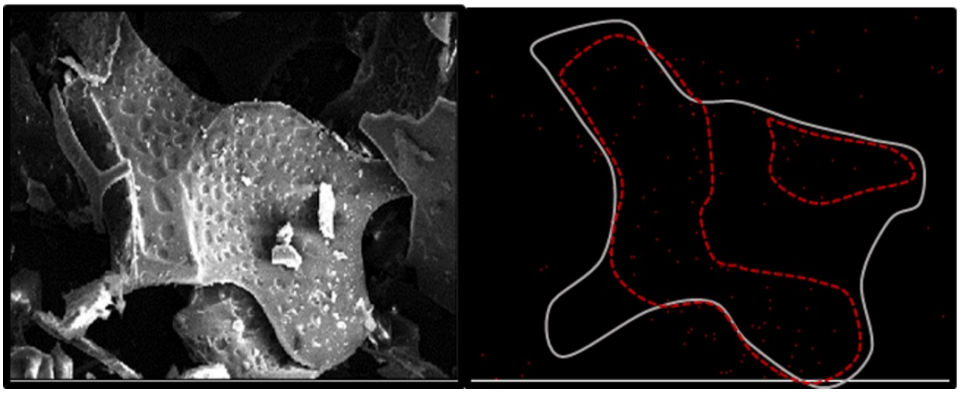

e

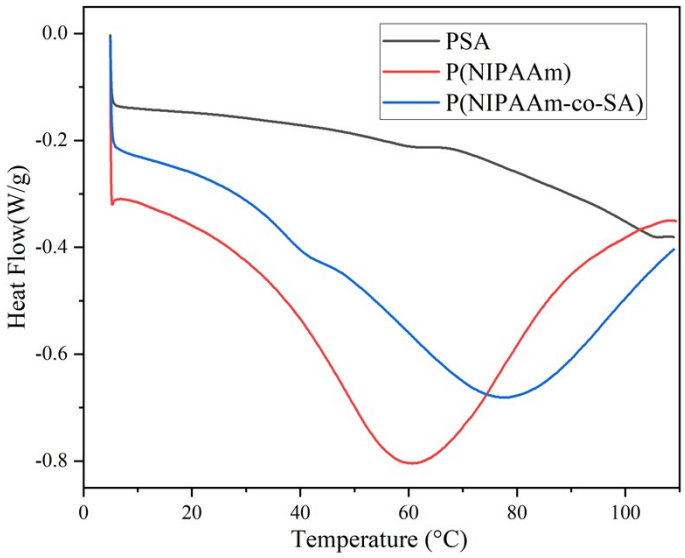
PSA
P(NIPAAm)
P(NIPAAm-co-SA)
Heat Flow(W/g)
Temperature (°C)
0.0
-0.2
-0.4
-0.6
-0.8
0
20
40
60
80
100

f

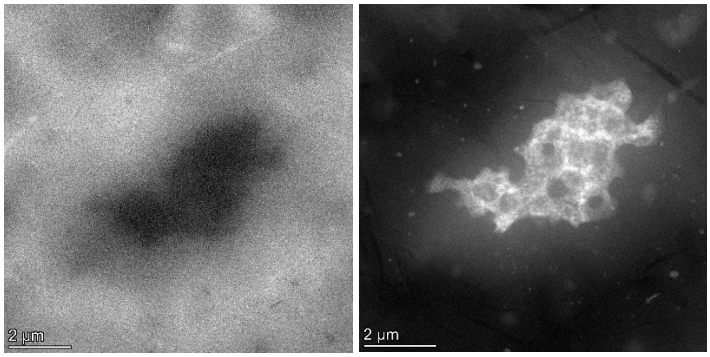
2 µm
2 µm

g

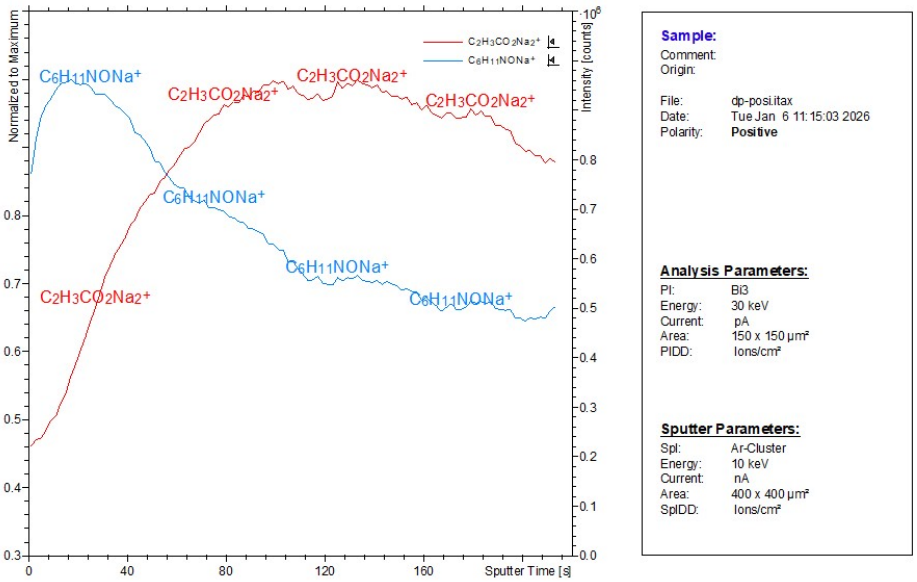
Normalized to Maximum
Intensity [counts]
Sputter Time [s]
C6H11NONa+
C2H3CO2Na2+
Sample:
Comment:
Origin:
File: dp-posi.itax
Date: Tue Jan 6 11:15:03 2026
Polarity: Positive
Analysis Parameters:
PI: Bi3
Energy: 30 keV
Current: pA
Area: 150 x 150 µm²
PIDD: Ions/cm²
Sputter Parameters:
Spl: Ar-Cluster
Energy: 10 keV
Current: nA
Area: 400 x 400 µm²
SplDD: Ions/cm²

Fig. S1. EDS mapping of Janus and uniform microgels. (a) J-3 with little P(NIPAAm) attached on the P(NIPAAm-co-SA) during the synthesis. (b) U-4 uniform microgels. (c) J-3 uniformly covered with P(NIPAAm). (d) J-3 with separated P(NIPAAm-co-SA) and P(NIPAAm) segments. (e) Baseline-corrected DSC thermograms (endotherm up) of PSA, P(NIPAAm), and P(NIPAAm-co-SA) (J-3) recorded during heating at 5 °C min^{-1}. (f) TEM and STEM figure of J-3 microgels. (g) ToF-SIMS depth profile (positive-ion mode) of J-3 microgels.

2. Experimental Setup for FO desalination

Fig. S22**.** displays the schematic and image of the FO setup. 2000 ppm by weight NaCl solution was used as feed solution to characterizate the performance of the Janus microgel[1,2]. The FO membrane, provided by Fluid Technology Solution. Inc, was clamped in between and the setup was well-sealed with the gasket clampping the FO membrane. The microgels, which were freeze-dried before the test, were placed on the FO membrane. There was a stirrer in the feed side that kept stirring the feed solution at a constant speed to avoid the accumulation of salt close to the FO membrane.

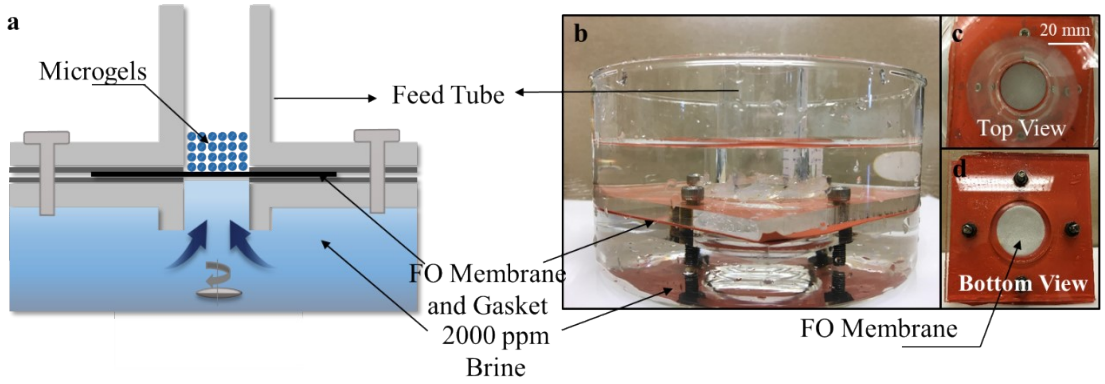

Fig. S2. Experimental setup for FO desalination: (a) Schematic and (b) photograph of the FO setup

3. Thermodynamic Limit of Energy Consumption

Fig. S3. demonstrates the color change of J-3 microgels as temperature increases. The microgel remained hydrophilic, indicated by the translucent state of the gels, when the temperature was ≤ 28 ℃. The microgels changed from the translucent state to the opaque one when the temperature reached 35℃ when the P(NIPAAm) switched from the hydrophilic state to hydrophobic one, as known as the LCST phase transition. The LCST of the Janus microgels is close the that for pure P(NIPAAm)[3,4], indicating that the ionic segment does not affect the intrinsic properties of thermos-responsive segments because it was not copolymerized with the P(NIPAAm) part.

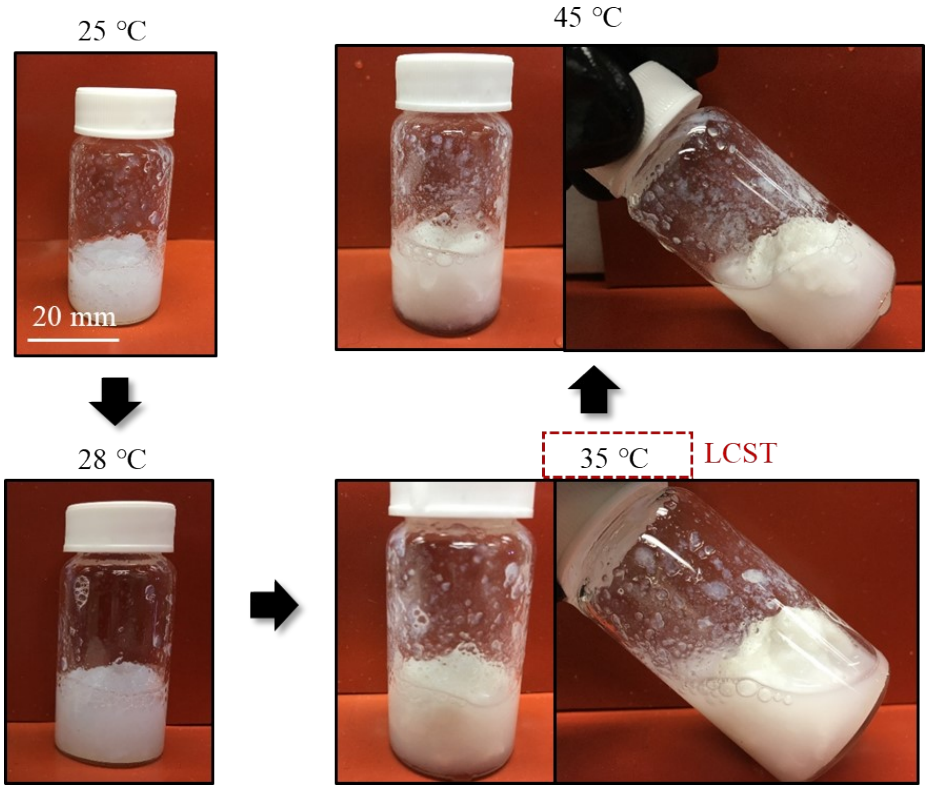

Fig. S3. Identification of LCST for J-3 Janus microgels

The LCST transition led to the fast deswelling of the microgels due to the hydrophobicity as shown in Fig. S3, where the dehydrated microgels tended to coagulated and were separated from the released water. It is noted that the water release ratio due to the LCST is independent of the temperature as long as the temperature is higher than the critical temperature[5,6] because it is a phase-transition instead of diffusion process. Due to the low LCST temperature (35℃) compared to that for other regeneration process, e.g., > 50 ℃ for membrane distillation to obtain flux of ~ 2 LMH [7], the Janus microgels enable a impactful energy saving for the regeneration process. It is reported that the LCST latent heat Q_L for P(NIPAAm) is around 42.25 kJ/kg$_{(NIPAAm)}$[8]. The sensible heat requirement can be calculated as:

$$Q_S = \int_{T_1}^{T_{LCST}} C_p dT \qquad \text{(S1)}$$

where C_p is the heat capacity with fixed pressure for water (4.2 kJ/kg·K) or P(NIPAAm) (1 kJ/kg·K on average from T_1=298 K ~ T_{LCST}=308 K) [3].

To obtain the specific latent heat in terms of mass of water, we estimate that the swelling ratio for J-3 is around 2 without considering the mass loss in recyclable FO process as shown in Fig. 6b.

And thus, the specific energy consumption for water production is ~ ***68 kJ/kg$_{(water)}$***, which is ***19 kWh/m^3$_{(water)}$*** as given by Eq.S2.

$$Q = Q_s^w + \frac{Q_s^{NIPAAm}}{2} + \frac{Q_L}{2} \tag{S2}$$

If the energy of desalinated water is recovered to heat up the feed solution, the energy consumption can be further reduced as shown in Eq. S3 assuming the reversible heat exchange process:

$$\int_{T_{LCST}}^{T_1} \frac{c_w}{T} dT + \int_{298}^{T_1} \frac{c_w}{T} dT = 0 \tag{S3}$$

The feed solution can be ideally pre-heated up to 303 K. And thus, the energy consumption can be reduced to ***13 kWh/m^3***. To further reduce energy consumption, one could extend the FO time or replace the P(SA) with more ionic polyelectrolytes to enlarge the swelling ratio.

Compared to the pure evaporation where the specific energy consumption is 611 kWh/m^3$_{(water)}$ as given by Eq. S4, the Janus microgel-based FO desalination enables an impactful energy saving even without considering the energy penalty for sensible heating and condensation.

$$Q_{evp} = h_{fg} \rho_w \tag{S4}$$

where h_{fg} is the latent heat of water and is 2200 kJ/kg; ρ_w is the density of water which is 1000 kg/m^3. More importantly, the low LCST temperature allows the direct utilization of solar energy as thermal input.

4. Water absorption kinetics

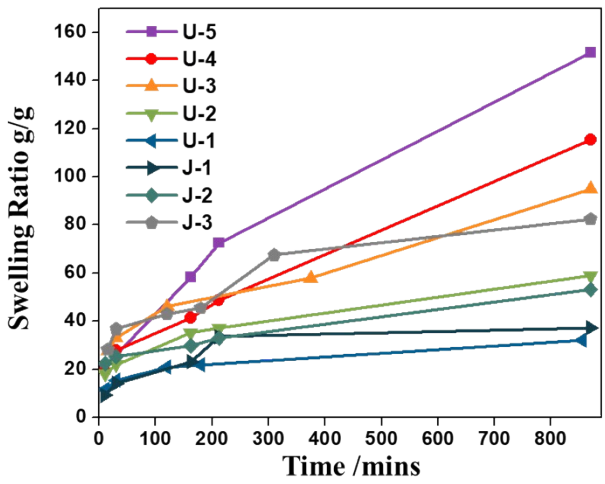

Fig. S4. Swelling ratio

It is apparent that the swelling curves for the uniform microgels can be delineated into two regions, i.e., the faster swelling stage at $t < 300$ mins and the slower swelling one afterwards. For example, the swelling ratio for the U-2 sample was ~ 36 g/g at $t = 200$ mins but it only increased to ~ 50 g/g at $t = 870$ mins. The swelling curve even plateaued for the U-1 after $t = 200$ mins. Although the swelling rate for the U-5 was also reduced after $t = 200$ mins, it still increased from ~ 75 g/g to ~ 143 g/g from $t = 200$ mins to 870 mins, which was much faster than other uniform gels. The reason is that both the swelling rate and osmotic pressure decrease as the microgel swells. With a higher SA concentration, the microgels can absorb more water before its osmotic pressure decreases and reaches an equilibrium with the feed solution. It is noted that the Janus microgel yielded a faster swelling rate than the uniform microgel with the same equivalent SA concentration. For example, the J-3 microgels swelled at the similar rate as that for the U-3, which was faster than that of the U-2 sample although the equivalent SA concentration for the J-3 (14%wt) was lower than that of the U-2 (23wt%).

5. Video of LCST phase transition and water release for J-3

See attachment.

6. Mechanism of salinity influence and the response of J-3 microgels

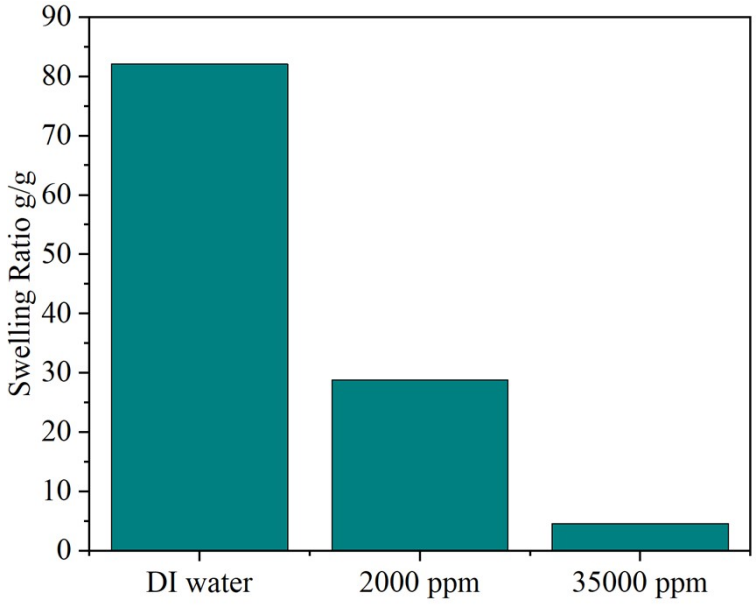

Fig. S5. Swelling ratio of the J-3 microgels under conditions of different salinity.

The osmotic pressure of seawater of 35000 ppm is 27 atm, which is significantly lower than that of P(SA) (100-200 atm). To calibrate the effect of osmotic pressure of solvent on the FO flux, the

swelling ratio of the microgels under high-salinity conditions (2,000 and 35,000 ppm) was measured. Admittedly, due to higher osmotic pressure in seawater, the swelling ratio decreased from 28.7 g/g to 4.6 g/g. which may lead to reduced FO flux. However, this can be arguably overcome by replacing the ionic segment in the current form into more ionically strong ones, e.g., using Poly(Magnesium Acrylate) where the osmotic pressure doubles by Mg^{2+} cation. We would like to highlight that our current work focuses on a generic framework to analyze the feasibility of thermoresponsive Janus microgels, which is material independent. Future research on new thermoresponsive and ionic segments following our design guidelines is highly desired, which however is out-of-the-scope of our current study.

7. An environmental life cycle assessment of the FO-thermal regeneration process

7.1. Objectives and scope of the FO-thermal regeneration system

(1) Forward osmosis thermal regeneration (FO-TR)

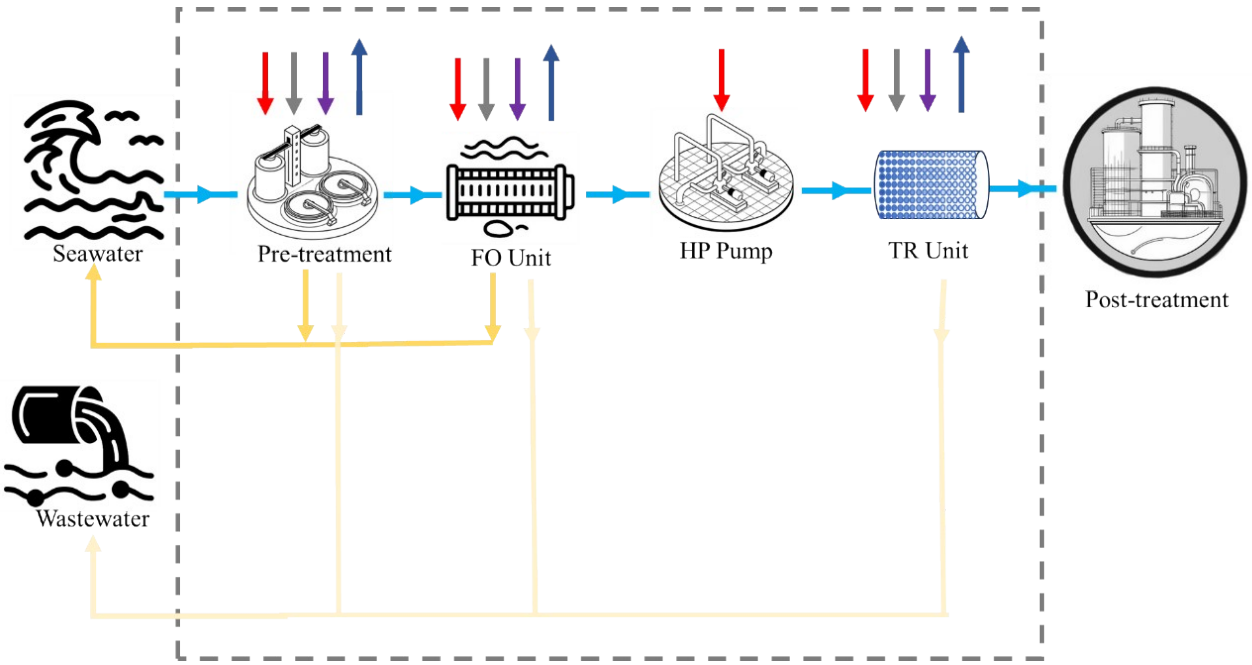

(2) Conventional Seawater Reverse Osmosis (SWRO)

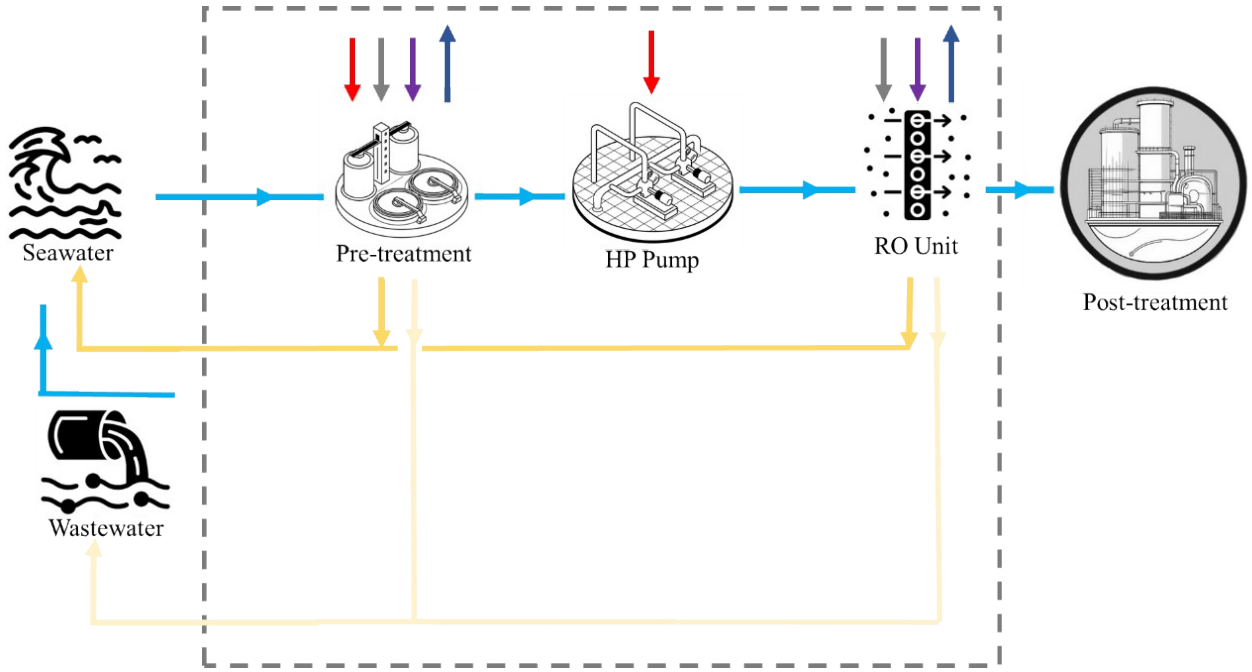

(3) Forward Osmosis-Reverse Osmosis Hybrid System (FO-RO)

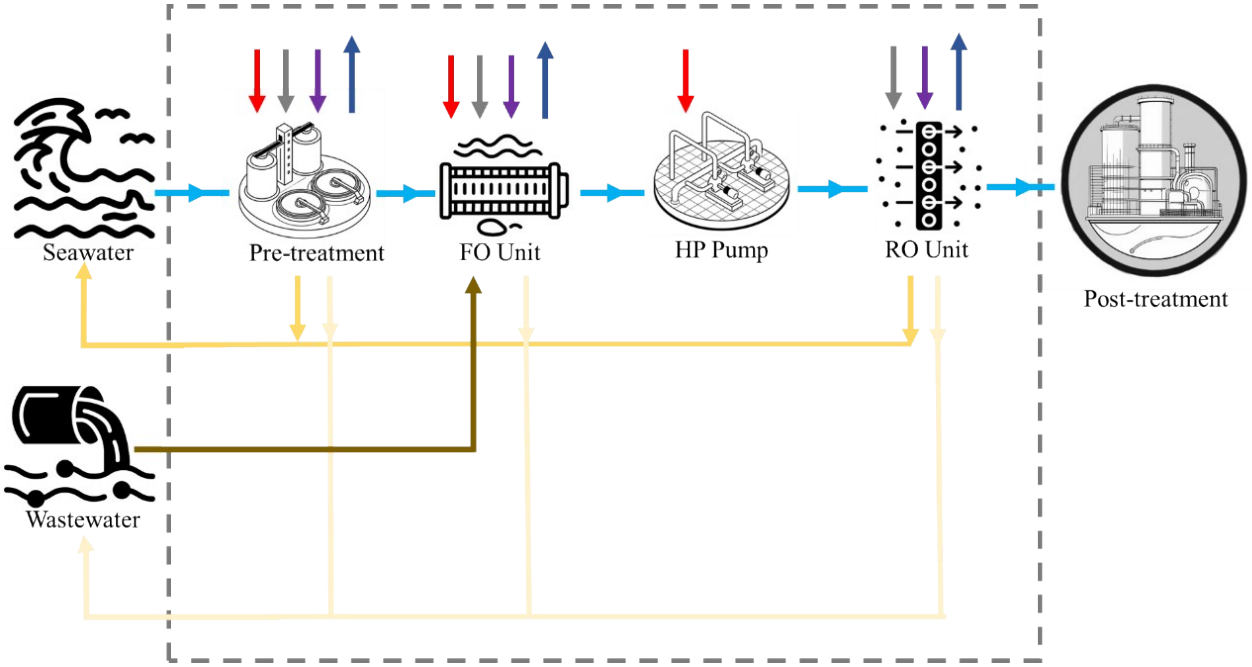

(4) Ultrafiltration-Reverse Osmosis Hybrid System (UF-RO)

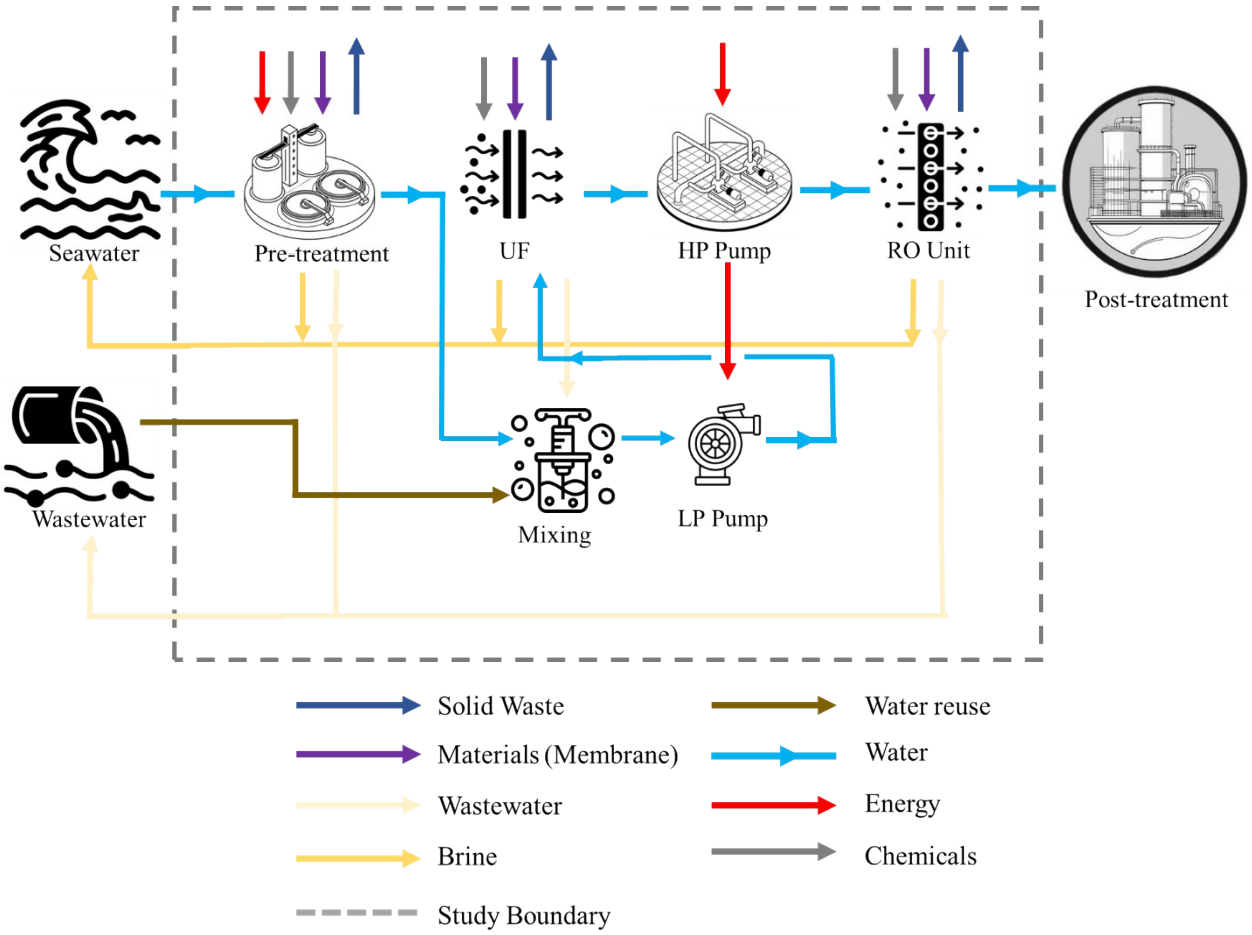

Fig. S6. Gate-to-grave LCI system boundaries and input, output flows for (1) Forward osmosis thermal regeneration (FO-TR); (2) Conventional Seawater Reverse Osmosis (RO); (3) Forward Osmosis-Reverse Osmosis Hybrid System (FO-RO), and (4) Ultrafiltration-Reverse Osmosis Hybrid System (UF-RO). Acronym: TR: thermal regeneration, HP: high pressure, LP: Low pressure, RO: reverse osmosis, FO: forward osmosis, UF: ultrafiltration.

The life cycle assessment (LCA) in this study focuses on the FO-thermal regeneration desalination system (Table S1). The functional unit is defined as 1 cubic meter of desalinated water produced by the system. The objective is to quantify the environmental impacts generated during the operational and disposal phases of the process and to identify the main sources of environmental burden. A "**gate-to-grave**" LCA approach is adopted, with the system boundaries illustrated in Fig. S6. Given that the service life of building structures, pipeline infrastructures, and large mechanical equipment typically far exceeds the operational period of the system, the environmental loads associated with their manufacturing and construction phases are relatively minor when amortized. Moreover, such phases are commonly excluded from system boundaries in relevant literature (e.g., Pazouki et al., 2021).[9] Therefore, they are also excluded from this analysis. Furthermore, findings

from Pazouki et al.[9] confirm that the environmental impacts of brine disposal and wastewater discharge are negligible, with their contributions being significantly lower than those from chemical consumption during membrane manufacturing, membrane cleaning (CIP) agents, and energy consumption. To enhance comparability with other systems, this study focuses the system boundary on material and energy consumption during the operational phase, as well as environmental loads from the end-of-life disposal phase. This includes chemicals used in CIP processes, consumption of membrane modules and draw agents, energy use, and waste disposal.

The main environmental loads during the operational phase include: (1) Chemical consumption: Regular membrane cleaning (CIP) and feedwater pretreatment require continuous inputs of chemicals such as acids, alkalis, chelating agents, and antiscalants, constituting a significant material flow burden; (2) Membrane module replacement: FO membranes have a limited life of service, assumed in this study to be 2000 cycles. The environmental interventions from the production and replacement of membrane materials, including polyamide active layers and support structures, are considered; (3) Draw Agents (DA): The synthesis and operation of DA involve certain material and energy inputs, particularly in high-osmotic-pressure systems. However, this study employs a solar-driven DA regeneration process, where the energy is derived from renewable thermal sources and does not incur additional environmental burdens. Thus, only the preparation and operational phases of the DA are included in the LCA; (4) Energy consumption: This primarily stems from hydraulic pumping processes, including seawater intake, recirculation in membrane processes, and DA regeneration and delivery. This study includes only electricity-driven pumping energy, excluding solar thermal energy and auxiliary system energy (Table S2). Some studies have used NH_3-CO_2 draw solutions and industrial waste heat for thermal-driven reconcentration, avoiding energy-intensive reverse osmosis processes and reducing the system's specific energy consumption (SEC) to 0.84 $kWh \cdot m^{-3}$, with 0.60 $kWh \cdot m^{-3}$ for reconcentration and 0.24 $kWh \cdot m^{-3}$ for recirculation pumps. Based on this, subsequent studies commonly adopt 0.25 $kWh \cdot m^{-3}$ as the reference FO energy consumption value excluding the reconcentration process, facilitating energy efficiency comparisons among systems[10].

Environmental loads during the disposal phase mainly include: (1) End-of-life treatment of membrane modules and draw agents: Decommissioned membranes and spent draw agents are assumed to be disposed of via sanitary landfill; (2) Waste liquid discharge: CIP waste generated

during membrane cleaning is treated as organic-load wastewater and directed to municipal sewage systems. The highly concentrated brine produced by the forward osmosis process is discharged directly into the ocean, which may pose potential impacts on coastal ecosystems, as shown in Fig. S6.

The FO-TR system modeled in this study, with a daily production capacity of 100 m^3, is suitable for distributed water supply scenarios in coastal cities. It is particularly well-adapted for integration with renewable energy sources, such as offshore wind and solar power.[11] The electricity required for system operation is supplied by an offshore wind power system, representing a desalination pathway driven by renewable energy.

7.2. Modeling for FO-TR process

We model a cyclic process in which a thermo-responsive hydrogel (draw agent) first absorbs water across a forward osmosis (FO) membrane from saline feed at ambient temperature, and then releases liquid water upon mild heating above its lower critical solution temperature (LCST). One cycle consists of four stages: FO absorption (at T_{amb}), heating, isothermal liquid-phase release (at T_{hot}), and cooling back to T_{amb}. Heating and release proceed concurrently (overlapped). The cycle must deliver a prescribed product volume V within a total time budget T_{cycle}. Here we present the governing equations, assumptions, and the optimization used to determine the minimal dry gel mass mg that achieves the target when the FO membrane area A_m and the initial FO flux parameter J_0 are fixed.

Assumptions: Above LCST the absorbed water is expelled as liquid; only sensible heats are considered. Constant specific heats $c_{p,g}$ (gel) and $c_{p,w}$ (water); constant temperature lift $\Delta T = T_{hot} - T_{amb}$. FO flux decays mono-exponentially in time; LCST release follows first-order approach-to-plateau. All hydraulic resistances and polarization effects are absorbed into the empirical flux parameters. The stage time is the maximum of heating time and release time; cooling is sequential. Osmotic driving force changes during absorption are captured implicitly by the flux model; a constant product density ρ_w is used for FO volume definitions.

Symbols: A_m (m^2): FO membrane area (fixed). J(t) (LMH): time-dependent FO water flux. J_0, J_∞, τ: FO flux parameters (initial, asymptotic, time constant). V(t) (L): cumulative absorbed volume

across FO by time t. m_g (g): dry mass of hydrogel (decision variable). w_2 (g/g): water/dry-gel mass ratio of swollen gel at the end of FO. f(t) (-): fraction of absorbed water released by time t at T_{hot}. f_{max}, k: LCST release plateau and rate constant. Q_{up}, Q_{down} (J): sensible heats for heating and cooling, respectively. A, η, I: illuminated area, solar-thermal efficiency, irradiance in Guangzhou, China. h, A_{ex}, ΔTc: cooling coefficient, exchange area, mean cooling temperature driving force. T_{cycle} (h): total cycle time budget; V (L): target product volume per cycle.

We represent the FO flux by a mono-exponential relaxation:

$$J(t) = J_\infty + (J_0 - J_\infty)e^{-t/\tau} \tag{S5}$$

With the standard FO definition of flux based on collected water mass, the cumulative absorbed volume is

$$J = \frac{m_t - m_0}{\rho_w A_m t} \Rightarrow V(t) = A_m \int_0^t J(t)dt \tag{S6}$$

$$V(t) = Am[J_\infty t + (J_0 - J_\infty)\tau(1 - e^{-t/\tau})] \tag{S7}$$

At T_{hot}, the fraction of the absorbed water that has been expelled as liquid by time t (minutes) is modeled as

$$f(t) = f_{max}(1 - e^{-kt}) \tag{S8}$$

For a given release duration t_{rel}, the released volume equals the released fraction of the swollen water contained in the gel:

$$m_{rel}(t_{rel}) = m_g \cdot w_2 \cdot f(t_{rel}) \tag{S9}$$

To meet the production target within one cycle we impose

$$m_g \cdot w_2 \cdot f(t_{rel}) = 1000\ kg \tag{S10}$$

The post-release water content that remains in the gel (entering cooling and the next FO stage) is

$$w_1 = w_2 \cdot [1 - f(t_{rel})] \tag{S11}$$

Let $\Delta T = T_{hot} - T_{amb}$. Heating the gel plus its swollen water from T_{amb} to Thot requires

$$Q_{up} = [m_g c_{p,g} + (w_2 m_g) c_{p,w} + c_{gel}]\,\Delta T \tag{S12}$$

Cooling the gel plus its residual water from T_{hot} back to T_{amb} requires

$$Q_{down} \approx [m_g c_{p,g} + (w_1 m_g) c_{p,w}]\,\Delta T \tag{S13}$$

Assuming solar–thermal input and Newtonian convective cooling,

$$t_{up} = \frac{Q_{up}}{\eta I A} \tag{S14}$$

$$t_{down} \approx \frac{Q_{down}}{h Ah\Delta T} \tag{S15}$$

According to Eq. (S12), calculate the amount of heat required to raise the temperature of 1 liter of fresh water during its production from the hydrogel. Assume the conditions in FO–TR process, T_{hot} =70 ℃, T_{amb}= 25 ℃, m_g=40 g, w_2=30 (g/g), $c_{p,g}$=1.0 kJ/(kg·K), $c_{p,w}$=4.12 kJ/(kg·K). Therefore, the heat required to raise the temperature of 1 liter of fresh water from the hydrogel is 230.29 kJ.

The solar radiation heat Q_{solar} received by the hydrogel can be calculated using the following formula：

$$Q_{solar} = I \cdot A \cdot t \cdot \gamma_{solar-thermal} \cdot \gamma_{availability} \tag{S16}$$

Where I (W/m²) is the solar radiation intensity, A is the effective area of the solar collector, and t is the radiation time. In the case of producing 1 liter of fresh water, assume that the solar radiation intensity I =1000 W/m², the effective area of the collector A =0.8 m², the radiation time t =18360 s (5.1 hour), $\gamma_{solar\text{-}thermal}$ =0.5, $\gamma_{availability}$ =0.5. Therefore, the usable solar radiation heat can be calculated to 4320 kJ.

In the FO–TR process, only the water absorbent recovery process requires the consumption of heat. Solar radiation under typical sunny conditions is sufficient to meet the heat required to heat the hydrogel (4320 kJ >230.29 kJ). Therefore, the FO–TR process can effectively utilize solar energy for water heating, demonstrating its potential application in heating absorbents.

7.3. Inventory analysis

The development of a Life Cycle Inventory (LCI) serves as the foundation and a critical prerequisite for conducting an Environmental Life Cycle Assessment (LCA). The compilation of LCI must adhere to the ISO 14040/14044 standards, ensuring clear data sources, well-defined system boundaries, consistent functional units, and adherence to mass balance between input and output flows.[12] To enable quantitative environmental impact analysis, this study imported input and output data from the system operation into **SimaPro (version 9.0.0.48)**, a dedicated LCA software, for

modeling and computation. The ***Ecoinvent v3*** emission factor database was employed to supplement data for upstream and downstream processes involved within the system boundary, particularly in handling energy and material flows imported into the technical system.

The LCI data for the FO-thermal regeneration system includes key input flows within the technical system boundary: raw materials (membrane module materials, absorbents), energy inputs (electricity), and auxiliary chemicals used during operation (such as cleaning and pretreatment agents). Output flows consist of end-of-life waste disposal (decommissioned membrane modules, spent absorbents) and emissions (concentrated brine, cleaning wastewater). These inventory flows form the foundational data for environmental impact assessment and are used in subsequent characterization analyses of impact categories. Furthermore, the relative mass and energy flows under various operating conditions, along with key design parameters, are summarized in Table S3.

Given limitations in database applicability and data availability, this study clearly distinguishes between foreground and background data during LCI construction. Foreground data were primarily obtained from experimental measurements and engineering design parameters, including membrane flux, energy consumption, absorbent dosage, and other input/output flows directly related to system operation. An upscaling methodology[13] was applied to extrapolate laboratory-scale data to industrial scale, ensuring that the forward-looking LCA maintains engineering applicability and practical representativeness, thereby reflecting the primary environmental interventions of the technical system. Background data were sourced from the ***Ecoinvent v3*** database to supplement upstream and downstream processes that are not directly observable, such as electricity production, membrane material manufacturing, chemical production, and waste stream treatment.

Since certain FO-related processes (e.g., absorbent production) lack direct corresponding modules in existing databases, some background data were approximated using functionally similar processes. Moreover, for key synthetic materials (such as absorbent precursor chemicals), this study separately modeled their production processes, thereby addressing gaps in database coverage. Relevant parameters and data sources are provided in Table S5 and Table S6 to enhance the accuracy and transparency of the LCI data, thereby providing more representative underlying input for environmental impact calculations.

To further quantify various environmental impacts, this study adopted the ***CML-IA baseline***

(V3.05 / EU25) method for impact classification and characterization. All environmental impact results were normalized and compared based on the functional unit (1 m^3 of water produced) to identify major sources of environmental burden and to support the optimization of the FO-thermal regeneration system (Table S7-Table **S10**).

Table S1. Technical design parameters determined for Forward osmosis thermal regeneration based on systems designed to produce 100 m^3/day of drinking water

Parameter	Value	Unit	Comment / Reference
System Type	FO-TR		Forward Osmosis system with thermal regeneration strategy
Design Capacity	100	m^3/day	Daily water production capacity of the system
Daily Operating Time	6	h/day	Assumed system operating time per day
Operation Lifetime	5	years	System expected lifespan (based on FO membrane lifespan)[9]
Feedwater Salinity (TDS)	32,000	mg/L	Initial seawater salinity
Brine Salinity (post-FO)	94,000	mg/L	Salinity of brine after FO treatment
Operating Temperature	25	°C	Operating temperature
Total Membrane Active Area	21,000	m^2	FO membrane area
Draw Agent	4,000	kg	Hydrogel
Draw Agent Lifetime	2000	cycles	Assumed full recovery and reuse without replacement
Design Water Flux	1	$L/m^2 \cdot h$ (LMH)	Design basis for membrane flux
Membrane Module Type	TFC-hollow fiber	–	Thin-Film Composite hollow fiber membrane

Table S2. Pumping Requirements and Energy Consumption in FO-TR System

Parameter	Seawater Intake Pump	FO Circulation Pump	Unit
Water Flow Volume	151.61	100	m^3/day
Number of Pumps	1	2	–
Daily Operating Time	6	6	h
Head (Pumping Lift)	40	10	m
Pump Efficiency	0.75	0.75	–
Water Density	1025	998.2	kg/m^3
Gravitational Acceleration	9.81	9.81	m/s^2
Pump Operation Time	21,600	21,600	s/day
Flow Rate	0.0100	0.0046	m^3/s
Pumping Power Requirement	3.76	0.60	kW
Daily Energy Consumption	22.59	3.63	kWh/day
Energy (1 m^3 of water produced)	0.2259	0.0363	kWh/m^3
SEC for FO System		**0.2984**	**kWh/m^3**

* In the FO system, the only energy consumption is pumping electricity, which is powered by offshore wind turbines.

Table S3. Operational phase of life cycle inventories (LCI) for the FO-thermal regeneration system for producing 1 m^3 (unit process) desalinated water

Chemical inputs	Value	Unit	Comments	Method
1.Pretreatment+ CIP (kg)	**5.30E-01**	**kg/m^3**		The pretreatment and CIP processes are assumed to be equivalent to those of the FO-RO system described in reference 9 .
Ferric chloride	1.80E-03	kg/m^3	Coagulation, Flocculation	
Sodium tripoly-phosphate $Na_5P_3O_{10}$	4.00E-03	kg/m^3	Antiscalants (Scale inhibitor)	
Sodium (meta) bisulphite	1.41E-02	kg/m^3	Dechlorination (oxidants scavengers)	Approximately using sodium sulfite due to similar chemical and functional properties. Both substances are sulfur-containing reducing agents commonly applied in water treatment, dechlorination, and corrosion control.
Sulphuric acids	4.59E-01	kg/m^3	pH adjustment, UF cleaning	
Hydrochloric acid (HCl) mix	3.50E-03	kg/m^3	Membrane cleaning (disk filter and membrane)	
Sodium hypochlorite	1.18E-02	kg/m^3	Membrane cleaning, Disk filter and UF, Biocide, chemically enhanced backwash (CEB)	
Na4EDTA, kg (x10-2) (or EDTA, ethylene di amine tetra acetic acid)	2.80E-02	kg/m^3	CTA FO cleaning	
Sodium hydroxide (100% caustic soda)	4.00E-03	kg/m^3	Membrane cleaning	0.002 kg of pure NaOH (100%) corresponds to 0.004 kg of a 50% NaOH solution.
Citric acid	9.30E-04	kg/m^3	Low pH, chemically enhanced backwash (CEB)	

Chemical inputs	Value	Unit	Comments	Method
Detergents	2.72E-03	kg/m^3	High pH	No specific data available for detergents (0.52% of total input). Approximation performed using alkaline cleaning agent (NaOH).
2. Draw Agent	**2.19E-02**			Based on experimental data and engineering estimates.
Hydrogel	2.19E-02	kg/m^3		
3. Membrane material	2.04E+00	**kg/m^3**		For processes involving only FO membranes, original values from reference 9 are used directly. For processes involving both FO and RO membranes, allocation is based on membrane area or mass ratio.
Polyester (PET) resin	1.02E-01	kg/m^3	RO Permeate Carrier, RO membrane substrate, FO draw channel spacer	
Polypropylene (PP)	1.06E+00	kg/m^3	FO/RO Feed channel spacer, Disk filter and UF membrane UF fiber (SWRO pre-treatment)	
Polyamide (PA)	3.17E-02	kg/m^3	FO/RO Membrane active layer	
Polysulfone (PSF)	1.12E-01	kg/m^3	FO/ RO membrane support layer	
Polyurethane (PU)	4.06E-01	kg/m^3	Gluing the membrane, potting of the UF hollow fiber membrane	
Polyvinylchloride (PVC)	3.31E-01	kg/m^3	FO sealant tape/ central collection of the module/ membrane housing, UF membrane housing (SWRO pre-treatment)	
Ethylene Propylene Rubber (ERP)	6.89E-05	kg/m^3	Brine Seal+ O-rings	EPR approximated by synthetic rubber.
Glass Filled Noryl	6.26E-05	kg/m^3	Interconnector	PPE approximated by polyamide (PA6/PA66) due to data unavailability and minor contribution.
4. Energy(kWh)	**2.98E-01**	**kWh/ m^3**		

Chemical inputs	Value	Unit	Comments	Method
Pump 1: FO membrane circulation pump (×2)	7.25E-02	kWh/ m^3		
Pump 2: Seawater circulation pump	2.26E-01	kWh/ m^3		
5. Waste to treatment				
Hydrogel	2.19E-02	kg/m^3	Hydrogel to sanitary landfill	
Disposed membrane (kg/m^3)	2.04E+00	kg/m^3	Disposed membrane to sanitary landfill	Plastic composite films are assumed to be disposed of via sanitary landfill.
CIP waste (m^3/m^3)	5.30E-04	m^3/m^3	CIP waste to sewer	Volume estimates are based on water density (1 kg/L).
Brine (TDS 94,000 mg/L)	5.16E-01	m^3/ m^3	Brine to ocean	Reference [9]

Table S4. Life cycle inventories (LCI) for producing 1 kg (unit process) hydrogel

Inputs	Value	Unit	Comments	Method
Chemical	**41.54**	**kg**		
SA	0.4	kg	Primary reactant, provides polymerizable monomers	Based on lab scale and reference [13]
NIPAAm	0.6	kg	Primary reactant, provides polymerizable monomers	
Deionized water	40.54	kg	Solvent	
Electricity/heat				
Electricity	2.19	kWh		

* Sodium acrylate (SA), isopropylacrylamide (NIPAAm)

Table S5. Life cycle inventories (LCI) for producing 40 kg sodium acrylate (SA)

Inputs	Value	Unit	Comments	Method
Chemical	**42.368**	**kg**		
Acrylic acid	41.76	kg	Primary reactant, provides polymerizable monomers	Reference[14]
Sodium hydroxide	0.608	kg	Neutralizes acrylic acid, adjusts pH to 7.5	
Electricity/heat				
Electricity	3.9	kWh	Drying (electricity)	

Table S6. Life cycle inventories (LCI) for producing 18.6 kg N-isopropylacrylamide (NIPAAm)

Inputs	Value	Unit	Comments	Method
Chemical	**177.1**	**kg**		

Inputs	Value	Unit	Comments	Method
Acrylonitrile	10.6	kg	Primary monomer	Reference[15]
Isopropanol	12.6	kg	Solvent, participates in reaction	
1, 4-hydroquinone	0.05	kg	Inhibitor, prevents undesired polymerization or side reactions	
Tetra-n-butyl ammonium chloride	0.20	kg	Phase transfer catalyst	Due to the minor quantity and lack of precise data for tetrabutylammonium chloride (0.15 kg, phase-transfer catalyst), the calculation was approximated using 0.2 kg of ammonium chloride
Water	130	kg	Extraction solvent	
Sulfuric acid	23.65	kg	Acidifying agent, promotes reaction	
Electricity/heat				
Electricity	1.8	kWh	Heating (thermal energy input)	

Table S7. Environmental impact categories and input parameters contribution for the FO-thermal regeneration system (unit process)

Impact category	Draw agents	Membrane material	CIP+Pre-treatment	Pump
ADP (kg Sb eq.)	7.54E-07	7.51E-06	1.43E-05	1.21E-07
ADPF (MJ)	1.99E+00	1.52E+02	5.84E+00	4.80E-02
GWP100a (kg CO_2 eq.)	1.02E-01	7.03E+00	2.79E-01	4.37E-03
ODP (kg CFC-11 eq.)	4.91E-09	2.44E-07	7.47E-08	2.36E-10
HT (kg 1,4-DB eq.)	3.49E-02	3.70E+00	2.74E-01	1.83E-02
FWAE (kg 1,4-DB eq.)	2.53E-02	4.24E+00	1.90E-01	9.13E-03
MAE (kg 1,4-DB eq.)	9.44E+01	7.39E+03	5.20E+02	1.07E+01
TE (kg 1,4-DB eq.)	1.02E-04	8.65E-03	8.92E-04	4.27E-05
POCP (kg C_2H_4 eq.)	3.60E-05	1.73E-03	2.07E-04	1.71E-06
AP (kg SO_2 eq.)	5.10E-04	2.51E-02	4.79E-03	2.47E-05
EP (kg PO_4^{3-} eq.)	1.82E-04	1.56E-02	9.12E-04	1.25E-05

* Method: CML-IA baseline V3.05 / EU25

*** Environmental impact categories**: ADP – abiotic depletion (kg Sb eq.); ADPF – abiotic depletion of fossil fuels (MJ); GWP100a – global warming potential over 100 years (kg CO_2 eq.); ODP – ozone layer depletion (kg CFC-11 eq.); HT – human toxicity (kg 1,4-DB eq.); FWAE – freshwater aquatic ecotoxicity (kg 1,4-DB eq.); MAE – marine aquatic ecotoxicity (kg 1,4-DB eq.); TE – terrestrial ecotoxicity (kg 1,4-DB eq.); POCP – photochemical oxidation potential (kg C_2H_4 eq.); AP – acidification potential (kg SO_2 eq.); EP – eutrophication potential (kg PO_4^{3-} eq.).

Table S8. Environmental impact categories and input parameters contribution for the Hydrogel (unit process)

Impact category	SA	NIPAAm	Deionized water	Electricity
ADP (kg Sb eq.)	2.07E-06	3.19E-05	1.52E-07	2.27E-07
ADPF (MJ)	1.92E+01	5.40E+01	4.25E-01	1.72E+01
GWP100a (kg CO_2 eq.)	9.54E-01	2.09E+00	3.69E-02	1.59E+00
ODP (kg CFC-11 eq.)	1.77E-08	1.19E-07	1.64E-08	7.15E-08
HT (kg 1,4-DB eq.)	2.08E-01	7.79E-01	2.52E-02	5.82E-01
FWAE (kg 1,4-DB eq.)	1.27E-01	4.11E-01	2.38E-02	5.94E-01
MAE (kg 1,4-DB eq.)	4.55E+02	1.33E+03	6.56E+01	2.46E+03
TE (kg 1,4-DB eq.)	6.00E-04	2.16E-03	2.65E-04	1.63E-03
POCP (kg C_2H_4 eq.)	1.26E-04	1.24E-03	1.00E-05	2.69E-04
AP (kg SO_2 eq.)	2.31E-03	1.37E-02	2.18E-04	6.99E-03
EP (kg PO_4^{3-} eq.)	6.29E-04	4.27E-03	1.13E-04	3.27E-03

* Method: CML-IA baseline V3.05 / EU25

Table S9. Environmental impact categories and input parameters contribution for the N-isopropylacrylamide (NIPAAm) (unit process)

Impact category	Acrylonitrile	Isopropanol	1, 4-hydroquinone	Tetra-n-butyl ammonium chloride	Water	Sulfuric acid	Electricity
ADP (kg Sb eq.)	4.19E-06	7.09E-06	3.63E-08	1.13E-07	4.11E-08	4.18E-05	1.05E-08
ADPF (MJ)	4.20E+01	3.92E+01	2.18E-01	1.85E-01	1.19E-01	7.38E+00	8.68E-01
GWP100a (kg CO_2 eq.)	1.71E+00	1.44E+00	1.01E-02	1.42E-02	1.06E-02	1.96E-01	9.78E-02
ODP (kg CFC-11 eq.)	8.97E-08	5.55E-08	5.62E-10	1.55E-09	3.68E-09	4.59E-08	7.11E-10
HT (kg 1,4-DB eq.)	4.12E-01	3.63E-01	2.52E-02	1.16E-02	5.72E-03	4.49E-01	3.19E-02
FWAE (kg 1,4-DB eq.)	1.83E-01	2.06E-01	4.18E-03	5.12E-03	4.90E-03	2.58E-01	2.34E-02
MAE (kg 1,4-DB eq.)	6.04E+02	6.88E+02	1.30E+01	1.62E+01	1.65E+01	7.24E+02	1.52E+02
TE (kg 1,4-DB eq.)	1.17E-03	1.03E-03	1.35E-05	2.72E-05	4.80E-05	1.22E-03	9.47E-05
POCP (kg C_2H_4 eq.)	2.92E-04	1.38E-03	6.22E-06	2.94E-06	2.40E-06	3.58E-04	1.61E-05
AP (kg SO_2 eq.)	8.13E-03	5.23E-03	3.93E-05	6.73E-05	5.06E-05	8.94E-03	4.32E-04
EP (kg PO_4^{3-} eq.)	4.63E-03	1.23E-03	1.66E-05	4.42E-05	2.12E-05	1.08E-03	9.52E-05

* Method: CML-IA baseline V3.05 / EU25

Table S10. Environmental impact categories and input parameters contribution for the sodium acrylate (SA) (unit process)

Impact category	Acrylic acid	Sodium hydroxide	Electricity
ADP (kg Sb eq.)	5.05E-06	9.80E-08	1.05E-08
ADPF (MJ)	4.69E+01	2.24E-01	8.75E-01
GWP100a (kg CO_2 eq.)	2.27E+00	2.06E-02	9.85E-02
ODP (kg CFC-11 eq.)	3.11E-08	1.24E-08	7.16E-10
HT (kg 1,4-DB eq.)	4.76E-01	1.23E-02	3.21E-02
FWAE (kg 1,4-DB eq.)	2.84E-01	9.63E-03	2.36E-02
MAE (kg 1,4-DB eq.)	9.51E+02	3.38E+01	1.53E+02
TE (kg 1,4-DB eq.)	1.34E-03	6.25E-05	9.54E-05
POCP (kg C_2H_4 eq.)	2.95E-04	4.04E-06	1.62E-05
AP (kg SO_2 eq.)	5.24E-03	1.01E-04	4.35E-04
EP (kg PO_4^{3-} eq.)	1.43E-03	4.69E-05	9.59E-05

References

1 D. Li, X. Zhang, J. Yao, Y. Zeng, G. P. Simon and H. Wang, *Soft Matter*, 2011, **7**, 10048.

2 D. Li, X. Zhang, J. Yao, G. P. Simon and H. Wang, *Chem. Commun.*, 2011, **47**, 1710.

3 Y. Lu, T. Chen, A. Mei, T. Chen, Y. Ding, X. Zhang, J. Xu, Z. Fan and B. Du, *Phys. Chem. Chem. Phys.*, 2013, **15**, 8276.

4 Mi Kyong Yoo, Yong Kiel Sung, S. C. Chong and M. L. Young, *Polymer*, 1997, **38**, 2759–2765.

5 M. K. Yoo, Y. K. Sung, Y. M. Lee and C. S. Cho, *Polymer*, 2000, **41**, 5713–5719.

6 Y. Pei, J. Chen, L. Yang, L. Shi, Q. Tao, B. Hui and J. Li, *Journal of Biomaterials Science, Polymer Edition*, 2004, **15**, 585–594.

7 D. Zhao, P. Wang, Q. Zhao, N. Chen and X. Lu, *Desalination*, 2014, **348**, 26–32.

8 A. Razmjou, Q. Liu, G. P. Simon and H. Wang, *Environ. Sci. Technol.*, 2013, **47**, 13160–13166.

9 P. Pazouki, H. R. Lu, A. El Hanandeh, W. Biswas, E. Bertone, F. Helfer and R. A. Stewart, *Desalination*, 2021, **504**, 114963.

10 S. Zou and Z. He, *Water Research*, 2016, **99**, 235–243.

11 G. Amy, N. Ghaffour, Z. Li, L. Francis, R. V. Linares, T. Missimer and S. Lattemann, *Desalination*, 2017, **401**, 16–21.

12 H.-J. Klüppel, *Int J Life Cycle Assessment*, 2005, **10**, 165–165.

13 F. Piccinno, R. Hischier, S. Seeger and C. Som, *Journal of Cleaner Production*, 2016, **135**, 1085–1097.

14 S. Khanlari and M. A. Dubé, *Journal of Macromolecular Science, Part A*, 2015, **52**, 587–592.

15 X. Chen and T. Okuhara, *Journal of Catalysis*, 2002, **207**, 194–201.